optica

Deterministic coupling of epitaxial semiconductor quantum dots to hyperbolic metamaterial

Y. D. Jang,[1] J. S. Baek,[1] V. Devaraj,[1] M. D. Kim,[1] J. D. Song,[2] Y. Wang,[3] X. Zhang,[3] and D. Lee[1,*]

[1]Department of Physics, Chungnam National University, Daejeon 34134, South Korea
[2]Center of Opto-Electronic Materials and Devices, KIST, Seoul 02792, South Korea
[3]Nanoscale Science and Engineering Center, University of California, Berkeley, California 94720, USA
*Corresponding author: dleee@cnu.ac.kr

Hyperbolic metamaterial (HMM) can enhance the radiative recombination rate of a near-field coupled emitter due to its large photonic density of states (PDOS). Thus far, this enhancement has only been demonstrated qualitatively on account of the difficulties to achieve an equal emitter–HMM distance as well as the same polarization for all emitters. Here, we report on the deterministic coupling of epitaxially grown quantum dots (QDs) with HMM, for which a quantitative investigation of the rate enhancement is possible. Advantages of epitaxial QDs over other emitters to investigate HMM coupling include a precise QD–HMM distance, the same polarization direction, and single-exponential decay of photoluminescence. In order to isolate metal-related effects, we have fixed the thickness of the silver (Ag) layer and have varied only that of the germanium (Ge) layer in the HMM to investigate the effect of the PDOS, which depends on the dispersion relation, which in turn depends on the thickness ratio. The recombination rate enhancement, as measured by lifetime reduction, varied from 2.2 to 4.2, depending on the thickness ratio of Ag and Ge in the HMM. These findings match well with simulation results, clearly supporting the role of HMM in the rate enhancement. The coupling of high-quality epitaxial QDs with HMM, demonstrated here for the first time, to the best of our knowledge, may bring about diverse future applications.   © 2018 Optical Society of America under the terms of the OSA Open Access Publishing Agreement

An anisotropic optical medium can be fabricated by alternately stacking metal and dielectric of deep sub-wavelength thicknesses. In certain configurations, the medium becomes a highly anisotropic hyperbolic metamaterial (HMM) with dielectric constants that are negative in one direction and positive in other directions [1]. A key distinction of HMM from other material systems having positive dielectric constants in all directions is its isofrequency surface, which is hyperboloidal and, therefore, supports infinite wavevectors (k) at a given frequency; as a result, the propagation of high-k modes is allowed through the HMM medium [2–5].

For a typical material, high-k modes are evanescent and cannot propagate in the medium; however, as evanescent waves with high-k values can propagate in HMM, the resulting greatly reduced information loss during the imaging of an object enables super-resolution imaging [6–8]. Such imaging of sub-wavelength sized objects has been reported with a cylindrically or spherically curved HMM structure [6,7]. In addition, the propagation of high-k modes in HMM leads to the realization of indefinite cavities with a resonant cavity having been demonstrated down to $\lambda/12$ [9–11].

Another important application is the enhancement of the spontaneous emission rate of an emitter induced by a strong coupling of emission to HMM modes [10]. Since HMM has a very large photonic density of states (PDOS) due to abundant high-k states coming from the hyperbolic dispersion curve, and the spontaneous emission rate of an emitter increases proportionally with PDOS, an emitter placed close to HMM can experience a strong spontaneous emission rate enhancement. This HMM-induced emission enhancement is spectrally broad due to its hyperbolic dispersion relation, which enables quantum nanophotonics applications [12].

Spontaneous emission rate enhancement using HMM has been reported with dye molecules [13,14] as well as colloidal quantum dots (QDs) [15,16]. A reduction in photoluminescence (PL) decay time from 2 ns on the dielectric to 1.1 ns on the HMM, as a result of HMM coupling, has been reported for dye molecules distributed in 20-nm-thick polymethyl methacrylate (PMMA) film [13,14]. However, considering that near-field coupling to HMM is highly sensitive to distance, decay time variations over 20 nm should be significant, thereby causing the measured decay curve to be the sum of numerous decay curves of different time constants. The random dipole direction of dye molecules or colloidal QDs additionally complicates any quantitative estimation of decay time and, therefore, the coupling strength of an HMM system, since HMM coupling strength is strongly polarization dependent. Due to these varied contributions, PL decay curves have often

been fitted with three (or two) decay components, making quantitative comparison difficult. Furthermore, close proximity of the emitters to the nearest metal layer of the HMM structure can make it hard to determine whether the reduced emitter lifetime is attributed to HMM coupling or to metal-related effects, such as quenching.

To demonstrate this key outcome of the HMM system indisputably, beyond the trend of qualitative treatments, we need to secure a quantitative agreement between theory and experiment, a task requiring a new system that takes care of the above-mentioned complications. An ideal emitter structure for a quantitative evaluation of rate enhancement due to HMM coupling should have the following characteristics: (i) a precisely defined distance between emitters and HMM, (ii) the same dipole direction for all emitters, (iii) single-exponential PL decay, and (iv) isolation of metal-related effects.

HMM coupling with epitaxial semiconductor QDs satisfies all of the above requirements for an ideal system. First, the epitaxial QDs are all located at the same distance from the top surface ($\Delta d < 1$ nm), since molecular beam epitaxy used for semiconductor QD growth can control the thickness of materials at monolayer resolution [17]. Second, epitaxial QDs, such as InAs QDs on GaAs, have dipoles all horizontally polarized due to a low aspect ratio. Third, high-quality epitaxial QDs are grown defect-free and well-isolated from each other [18], such that carrier decay in the QDs is single-exponential, as long as the excitation power is low enough to have only excitons in the ground state [19]. This enables an accurate and clear determination of the emission rate enhancement by HMM coupling. Additionally, once excitons are generated in the QD, they are all converted to photons [20] due to the good isolation property of QDs, providing almost 100% quantum efficiency. In terms of fabrication, the epitaxial QD epilayer has an atomically flat top surface, so that high-quality HMM deposition is possible directly on top of the QD epilayer. To address the fourth requirement, we investigate HMM coupling effects with epitaxially grown QDs by varying the thickness of the germanium (Ge) layer, while that of silver (Ag) and the distance between the QDs and metal layer are kept the same. With this combination, any metal-related effects should be well-isolated, since the metallic effects will be the same for all samples such that any variation will mainly result from the difference in HMM coupling strength.

Finite difference time-domain (FDTD) simulation is carried out to estimate the HMM coupling of InAs QD emission. In the simulation, the thickness of each metal layer in the HMM is fixed to isolate metal effects, while the thickness of the dielectric material is varied. The observed QD exciton lifetime variation should then originate from the difference in coupling strength to the HMM.

Ag and Ge are chosen for the HMM, since the pair gives a significant change in Purcell enhancement factor (PF) on dielectric thickness. HMM is a highly anisotropic medium, in which one of its dielectric constants becomes negative in a specific direction. According to the effective medium theory, effective dielectric tensors are defined as follows [10]:
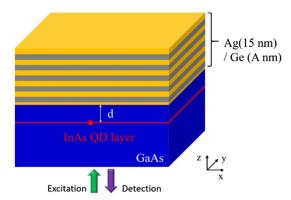
$$\varepsilon_{xx} = \varepsilon_{yy} = \frac{\varepsilon_m d_m + \varepsilon_d d_d}{d_m + d_d}, \qquad \frac{1}{\varepsilon_{zz}} = \frac{d_m/\varepsilon_m + d_d/\varepsilon_m}{d_m + d_d}, \quad (1)$$

where $\varepsilon_{xx} = \varepsilon_{yy}$ and ε_{zz} are the effective dielectric constants in-plane and normal to the layers, respectively, d_m and d_d are metal

and dielectric thicknesses, respectively, and ε_m and ε_d are the dielectric constants of metal and dielectric layers, respectively. For the type II HMM condition ($\varepsilon_{zz} > 0$ and $\varepsilon_{xx} < 0$), the dielectric-to-metal thickness ratio is $-\varepsilon_d/\varepsilon_m < \delta d(= d_d/d_m) < -\varepsilon_m/\varepsilon_d$, providing thickness ratios ranging from 0.36 to 2.75 for the Ag/Ge HMM at 1030 nm.
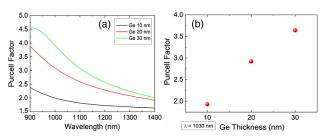
The thickness of Ag is maintained at 15 nm, while the thickness of Ge varies from 10 to 30 nm. In-plane polarized dipoles (QDs) are positioned 18.4 nm below the HMM, including a 2 nm Ge layer; this distance is chosen to be close enough to achieve strong coupling, but far enough not to generate defects near the QDs (see Supplement 1). The target wavelength is set to 1030 nm, at which the employed InAs/GaAs QDs emit. Five periods of alternating Ag and Ge layers build the HMM, as shown in Fig. 1.

FDTD simulations are carried out with FDTD Solutions (Lumerical Inc.). The mesh size normal to the HMM is set to 0.5 nm in the HMM region and to 1 nm in all directions in the dipole emitter region. PF is obtained from the ratio of total transmission through a 10 nm × 10 nm × 10 nm monitor box surrounding an emitter located near the HMM to that for an emitter in free space (see Supplement 1). The dielectric functions for Ag are from Johnson and Christy [21].

Simulated PF spectra and PF values at 1030 nm are plotted as a function of Ge thickness at a fixed Ag thickness of 15 nm in Fig. 2. The PF is significantly larger for HMM samples with

Fig. 1. Schematic of the HMM-coupled QD structure under consideration. The green arrow indicates excitation direction, and the purple arrow shows the measurement direction. A thin Ge layer of 2 nm is deposited before HMM deposition.

Fig. 2. (a) PF spectra simulated by the FDTD method and plotted as a function of Ge thickness with Ag thickness fixed at 15 nm. (b) PFs of QD emission as a function of Ge thickness at 1030 nm. A dipole emitter is positioned 18.4 nm below the HMM composed of five periods of Ag (15 nm)/Ge (A nm) layers.

thicker Ge layers at all wavelengths [Fig. 2(a)], and its value varies from 1.9 for a Ge thickness of 10 nm to 3.6 for a 30-nm-thick Ge layer at 1030 nm [Fig. 2(b)]. This difference is largely due to the smaller $dk/d\omega$ and the larger minimum ky for the 10 nm Ge sample (see Supplement 1). As a result, the radiative recombination time, which is inversely proportional to the corresponding PF, is expected to be significantly shorter for the samples with thicker Ge layers. Note that the thickness of the metal layer and the QD–metal distance are kept the same here, so that variation is mainly due to differences in HMM geometry.

In this work, we utilize epitaxial InAs/GaAs QDs in GaAs, grown by molecular beam epitaxy [22]. The InAs QD has 50-nm-thick GaAs capping, with a diameter of ∼25 nm and height of 4 nm, and emits light at 1030 nm at 12 K. Epitaxially grown semiconductor QD samples have sub-nanometer surface roughness as a consequence of layer by layer growth, which is important when we precisely define the distance between the QDs and HMM. Wet chemical etching is employed to decrease the QD surface distance, such that the QD–HMM distance is close enough to enable strong coupling. The HMM is able to be directly deposited on the flat etched surface of the QD sample.

The Ag and Ge layers should be flat in an HMM structure, so magnetron sputtering is employed, and its parameters are optimized for both flat Ag and Ge thin films [23]. Surface roughness in the optimized layer is measured to be 0.86 nm [root mean square (RMS) value] for the 10-nm-thick Ge surface and 0.97 nm for the 15-nm-thick Ag surface. A 2-nm-thick Ge wetting layer is deposited on the QD sample surface prior to the first Ag deposition for a better Ag film [24].

As QD emission couples to HMM through near-field coupling with exponentially decreasing strength for increasing QD–HMM distance, the QDs should be located close enough to the HMM for effective coupling. However, when QDs are placed too close to the HMM, QD emission quenching may become serious, and defects may develop around the QDs due to strain relaxation; here, the InAs/GaAs QDs are highly strained, such that the strain can be relaxed if the GaAs capping layer is too thin, which deteriorates QD emission properties. Therefore, we need to find the optimal distance between the QDs and HMM that achieves strong coupling, while also maintaining good QD emission characteristics. Determined by PL measurements from QD samples of different capping layers, a QD–HMM distance of 18.4 nm is chosen, since it is thick enough not to induce strain relaxation, but thin enough to provide for good coupling (see Supplement 1).

With the distance fixed at 18.4 nm, three different configurations of HMM are prepared to check the predicted PFs by FDTD simulation. The 50-nm-thick top side of the QD epilayer is etched to 16.4 nm by wet chemical etching. Thin Ag and Ge layers are alternatively deposited for five periods on the etched surfaces of the QD samples. The thickness of each Ag layer is kept to 15 nm, at which a flat surface is reliably obtainable with our optimized deposition condition [23], and that of the Ge layer is varied from 10, 20, and 30 nm. PL spectra are taken from the GaAs substrate side (see Fig. S3 in Supplement 1), since the PL of high-k modes cannot escape from the HMM. The excitation wavelength is chosen to be 850 nm, at which the GaAs substrate is transparent, but the QDs can still be excited. PL decay time (i.e., exciton lifetime) is measured by a picosecond streak camera (Hamamatsu C1587) with 150 fs pulse excitation at 850 nm.
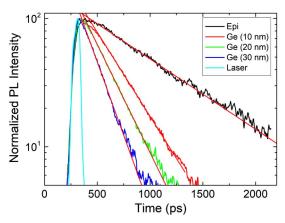
Strong HMM coupling of QD emission should enhance the QD emission rate, which can be revealed through a shortening of exciton lifetime in experiment. When the decay time of QD emission decreases because of the emission rate enhancement, uncoupled emission directed to the substrate will also experience the same lifetime shortening since they share the same emitters (excitons in the QDs). Therefore, HMM coupling of QD emission can be examined by substrate-side QD PL.

The measured PL transients from QDs coupled to HMM are plotted for different Ge thicknesses in Fig. 3. The decay curve from the original QD epilayer, without HMM deposition, is also included for comparison. All decay transients are single-exponential, which is typical for epitaxial QDs at sufficiently low excitation [19]; this is a key advantage of the present system, which enables a simple comparison of decay rates. Moreover, the single-exponential decay is maintained, since the QD–HMM distance is the same for all QDs, and QD polarization is in-plane. Otherwise, the final PL decay curve would be a linear combination of many single-exponential decay curves of different time constants, resulting in non-single-exponential decay from which it is difficult to extract a relevant component.
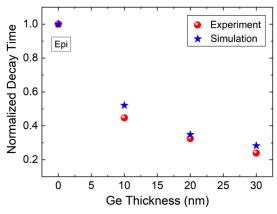
The PL decay times are significantly shorter for the HMM-deposited QD samples than that of the original QD sample, which attests to the recombination rate enhancement of QD excitons caused by strong HMM coupling. In addition, the decay transient is faster with larger Ge thickness, ranging from 10 to 30 nm, suggesting stronger coupling for thicker Ge samples. The measured decay curve is fitted by a single-exponential function, as shown in Fig. 3, with the following results: 790, 355, 255, and 190 ps for the original, 10–, 20–, and 30-nm-thick Ge HMM–QD samples, respectively.

Measured exciton lifetime as a function of Ge thickness is compared with the one calculated by the FDTD method at each PL peak wavelength in Fig. 4. Since exciton lifetime is inversely proportional to the corresponding PF when its quantum efficiency is close to 1, like our QDs, the inverse of the simulated PF is the corresponding calculated exciton lifetime. The decay times and PFs are normalized to the decay time (790 ps) and PF (1) of the original QD sample, respectively.

The experimental decay time as a function of Ge thickness shows a good match with the calculated PF variation, which

Fig. 3. Measured PL transients from the HMM samples with different Ge thickness (10, 20, and 30 nm). Epi indicates PL decay from an original QD sample, and Laser is for instrument response function.

Fig. 4. Comparison of the measured lifetimes of QD exciton (normalized to the value of bare QDs, 790 ps) and the calculated lifetimes for different Ge thickness samples.

indicates that the shortened exciton lifetime is indeed due to the increased HMM coupling of QD excitons. In our measurements, as the thickness of the Ag layer is fixed to isolate metal-related effects so that lifetime and PF variations result solely from structural differences in the HMM, the present experimental verification for the predicted consequence of HMM is highly reliable.

The stronger coupling in the 30 nm Ge HMM likely stems from more available high-k modes than the other HMM samples, as shown in the dispersion curves by FDTD simulation (see Fig. S4 in Supplement 1). The experimental result matches well with the FDTD calculation, attesting to the role of high-k modes in the HMM. The propagation of high-k modes supports QD emission coupling to the whole HMM and not just to the nearest metal layer.

We have *quantitatively* investigated the coupling of epitaxial QDs with HMM by measuring the radiative recombination rate enhancement of the QDs. The QD is ideal to study HMM coupling, since it has the same QD–HMM distance within 1 nm for all QDs, the same polarization direction for all QDs, and single-exponential decay of the PL signal. To further reduce uncertainties, we have isolated metal-related effects by keeping the Ag thickness the same and varying only that of Ge in the HMM. The recombination rate enhancement, observed through lifetime reduction, shows a clear difference between HMMs: 4.2 for the 15 nm Ag/30 nm Ge, and 2.2 for the 15 nm Ag/10 nm Ge. The result matches well with FDTD simulation results, clearly supporting the role of HMM in the rate enhancement. We believe that this demonstration of HMM coupling with the extensively studied epitaxial QDs may bring many novel applications.

See Supplement 1 for supporting content.

REFERENCES

1. S. Foteinopoulou, E. N. Economou, and C. M. Soukoulis, Phys. Rev. Lett. **90**, 107402 (2003).
2. A. A. Orlov, P. M. Voroshilov, P. A. Belov, and Y. S. Kivshar, Phys. Rev. B **84**, 045424 (2011).
3. A. V. Chebykin, A. A. Orlov, A. V. Vozianova, S. I. Maslovski, Y. S. Kivshar, and P. A. Belov, Phys. Rev. B **84**, 115438 (2011).
4. L. F. Shen, T. J. Yang, and Y. F. Chau, Phys. Rev. B **77**, 205124 (2008).
5. J. Schilling, Phys. Rev. E **74**, 046618 (2006).
6. J. Rho, Z. Ye, Y. Xiong, X. Yin, Z. Liu, H. Choi, G. Bartal, and X. Zhang, Nat. Commun. **1**, 143 (2010).
7. Z. Liu, H. Lee, Y. Xiong, C. Sun, and X. Zhang, Science **315**, 1686 (2007).
8. A. Salandrino and N. Engheta, Phys. Rev. B **74**, 075103 (2006).
9. X. Yang, J. Yao, J. Rho, X. Yin, and X. Zhang, Nat. Photonics **6**, 450 (2012).
10. A. Poddubny, I. Iorsh, P. Belov, and Y. Kivshar, Nat. Photonics **7**, 948 (2013).
11. J. Yao, X. Yang, X. Yin, G. Bartal, and X. Zhang, Proc. Natl. Acad. Sci. USA **108**, 11327 (2011).
12. Z. Jacob, I. I. Smolyaninov, and E. E. Narimanov, Appl. Phys. Lett. **100**, 181105 (2012).
13. J. Kim, V. P. Drachev, Z. Jacob, G. V. Naik, A. Boltasseva, E. E. Narimanov, and V. M. Shalaev, Opt. Express **20**, 8100 (2012).
14. Z. Jacob, J. Y. Kim, G. V. Naik, A. Boltasseva, E. E. Narimanov, and V. M. Shalaev, Appl. Phys. B **100**, 215 (2010).
15. H. N. Krishnamoorthy, Z. Jacob, E. Narimanov, I. Kretzschmar, and V. M. Menon, Science **336**, 205 (2012).
16. H. N. S. Krishnamoorthy, Z. Jacob, E. Narimanov, I. Kretzschmar, and V. M. Menon, in *Quantum Electronics and Laser Science Conference (QELS)* (2010).
17. D. Leonard, M. Krishnamurthy, C. M. Reaves, S. P. Denbaars, and P. M. Petroff, Appl. Phys. Lett. **63**, 3203 (1993).
18. D. J. Mowbray and M. S. Skolnick, J. Phys. D **38**, 2059 (2005).
19. Y. D. Jang, E. G. Lee, J. S. Yim, D. Lee, W. G. Jeong, S. H. Pyun, and J. W. Jang, Appl. Phys. Lett. **88**, 091920 (2006).
20. E. G. Lee, M. D. Kim, D. Lee, and S. G. Kim, J. Appl. Phys. **98**, 073709 (2005).
21. P. B. Johnson and R. W. Christy, Phys. Rev. B **6**, 4370 (1972).
22. M. D. Kim, S. K. Noh, S. C. Hong, and T. W. Kim, Appl. Phys. Lett. **82**, 553 (2003).
23. V. Devaraj, J. Lee, J. Baek, and D. Lee, Appl. Sci. Converg. Technol. **25**, 32 (2016).
24. W. Chen, M. D. Thoreson, S. Ishii, A. V. Kildishev, and V. M. Shalaev, Opt. Express **18**, 5124 (2010).